JOURNAL OF MATERIALS SCIENCE 24 (1989) 3053–3058

Preparation of amorphous Fe–Zr alloys by mechanical alloying and melt spinning methods

Part 1 *A structural comparison*

G. ENNAS, M. MAGINI*, F. PADELLA, P. SUSINI
Amorphous Materials Project, Chemistry Sector, ENEA, CRE-Casaccia, Via Anguillarese, Rome, Italy

G. BOFFITTO
Saes-Getters S.p.A., Via Gallarate 215, Milano, Italy

G. LICHERI
Chemistry Department, Universita' di Cagliari, Via Ospedale 70, Cagliari, Italy

Amorphous iron–zirconium alloys have been obtained by mechanical alloying (MA) starting from either pure elemental powders or from intermetallic compounds. X-ray diffraction was used in monitoring the amorphization process. Differences in the amorphization kinetics have been detected for the two different starting situations. The possibility of obtaining totally amorphous samples when starting from intermetallic compounds has been discussed. Amorphous iron–zirconium ribbons were also obtained by the classical melt-spinning (MS) method. A detailed structural comparison of the radial distribution functions led to the conclusion that the arrangement of the first neighbours is indistinguishable in the amorphous samples prepared by MA and MS methods.

1. Introduction

Mechanical alloying (MA) is a high-energy ball-milling technique known from the seventies and successfully exploited in industrial powder metallurgy to produce dispersion-hardened superalloys [1, 2]. Later it was observed that the method could be used to produce amorphous alloys starting from elemental powders [3]. Since then, amorphous alloy preparation by MA has been a subject of increasing interest in the literature [4, 5], due to the fact that both scientific and technological [6] aspects are joined in this preparative method.

In the mechanisms of the amorphization process, several arguments have been pointed out. In a careful study of the Ni–Ti system, Schwarz *et al.* [7] indicate that the process proceeds via the formation of elemental layers of the starting powders, accompanied by a solid state interdiffusion reaction. Two main requirements should be fulfilled: (a) large negative enthalpy of mixing of the alloying elements, and (b) anomalous fast diffusion of one element into the other. On the other hand, Thompson and Politis [8] were able to prepare Ti–Pd amorphous alloys and no fast diffusion of one component into the other exists. In fact, the debate is open and any contribution may be of help in elucidating the basic features of the amorphization process.

Concerning structural aspects, very little has been done. Enzo *et al.* [5] have examined amorphous mechanically alloyed Ni_{50}–Ti_{50} by radial distribution analysis (X-ray and extended X-ray absorption fine structure, EXAFS). Systematic structural investigations are lacking; above all, comparison of samples of the same composition prepared by the classical melt-spinning (MS) method and MA are practically absent.

The iron–zirconium system has been largely investigated, probably for its technological aspects, when prepared by the MS method (see e.g. [9–11]). Recently, a good deal of work has also been done on samples prepared via MA starting from pure elemental powders [12–15].

In this paper we present results on amorphous iron–zirconium alloys obtained by MA either from pure elemental powders and from commercial alloys of the same composition containing intermetallic compounds. Structural information has been inferred through radial distribution functions and detailed structural comparison between melt-spun ribbons and mechanically alloyed powders has also been carried out.

2. Experimental procedure

2.1. Sample preparation and analysis

For MA samples, pure iron (99.999%) and zirconium (99.9%) (iron from Carlo Erba; zirconium from Ventron GmbH; particle size 5 to 40 μm) were mixed to the average compositions $FeZr_2$ and Fe_2Zr. Commercial crystalline alloy of $FeZr_2$ composition, produced by Saes-Getters company, was used as starting

*Author to whom all correspondence should be addressed.

0022–2461/89 $03.00 + .12

materials for both the MS and MA preparative methods. The Saes-Getters alloy (hereafter saes) was prepared by melting the components in an induction furnace under vacuum (10^{-3} mbar) and then transferred, in vacuum, to a mould. Room temperature was reached by following thermal inertia. The ingot was comminuted by milling for about 1 h. Saes powder of $\sim$ 100 mesh was sieved for MA while grains from 1 to 5 mm were chosen for MS. The oxygen content was checked in all starting materials by standard LECO RO-17 equipment and never exceeded 1%.

The MA process was carried out in a conventional planetary ball mill (Fritsch "Pulverisette") using cylindrical tempered steel vials provided with a stop cock and a ball-to-powder weight ratio of approximately 10:1. To avoid oxidation, the vial was sealed under pure argon containing less than 1 p.p.m. oxygen. Several trials were performed in order to optimize the milling procedure. Milling for 1 h consisted of four intervals of 15 min each followed by 30 min rest to avoid excessive warming of the vials. The vials were opened from time to time for X-ray monitoring. Care was taken in order to remove homogeneous samples. The typical orange skin around the balls, indicative of multilayer formation, was observed during the early milling stages.

Melt-spun ribbons were prepared under vacuum (10^{-3} mbar) and with an overpressure of 100 mbar using the MS apparatus (Model 7400) from Buhler Company. Quartz crucibles with a 1 mm hole were used. Spinning was performed at 40 m sec^{-1} wheel speed and totally amorphous ribbons of $\sim 50\ \mu$m were obtained. Changing spinning conditions resulted in partially crystallized ribbons which were also analysed for comparative purposes.

Analytical controls were performed on final amorphous samples and no composition variations were detected. Oxygen content amounted at a maximum of 3% in MA samples after 60 h of milling.

The densities of all MA samples were obtained by heliostereopicnometry (Quantachrome Mod. SPY-2). A Westhphal balance was used for the ribbons and the starting saes alloy. The results are summarized in Table I.

2.2. X-ray data collection and treatment

Qualitative X-ray spectra of the starting materials and of the milled powders were recorded by an automatic Seifert diffractometer (PAD II) using Mo$K\alpha$ radiation. Quantitative data collection for radial distribution functions were carried out by a θ–θ X-ray diffractometer already described [16]. Intensity data were collected with Mo$K\alpha$ radiation at discrete intervals with a narrow advancement step so that about 400 points covered the whole explored angular range (from 2° to 70° θ corresponding to $s = 4\pi \sin\theta/l$ from 6 to 160 nm^{-1}). Usual data treatment followed [16]. However, owing to the high amount of zirconium present in the samples, a zirconium filter of 0.08 mm was inserted between them and the X-ray tube to avoid fluorescence radiation. Even so, residual background of the source excited fluorescence radiation from the samples which was removed by following a procedure already described [16]. The observed intensities, corrected for absorption and polarization, were normalized to a unit of volume, V, containing one iron atom. The structure function $i(s)$ were obtained according to

$$i(s) = \left[I_{\text{c.u.}} - \sum n_i f_i^2(s) \right]$$

where $I_{\text{c.u.}}$ are normalized intensities, n_i are stochiometric coefficients of the assumed unit, and $f_i(s)$ are the scattering factors of the species.

Radial distribution functions, $D(r)$, were calculated according to

$$D(r) = 4\pi r^2 \varrho_0 + 2r/\pi \int_{s_{\min}}^{s_{\max}} si(s)M(s) \sin(rs)\, ds$$

TABLE I Densities of the investigated samples. Westhpal balance and heliostereopicnometry measurements are indicated by W and H, respectively. Saes alloy is the starting alloy both for MS and MA samples

Sample	Density (g cm^{-3})	
	W	H
$FeZr_2$-commercial alloy	6.95 (2)	7.03 (5)
$FeZr_2$-MS	6.83 (1)	–
$FeZr_2$-MA (mix)	–	6.87 (5)
$FeZr_2$-MA (saes)	–	6.94 (5)
Fe_2Zr-MA (mix)	–	7.25 (5)

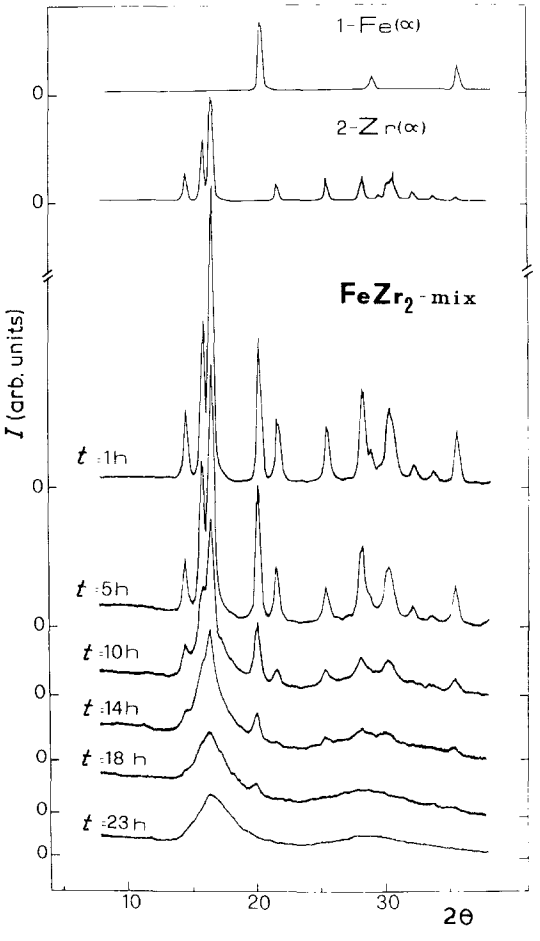

Figure 1 X-ray diffraction patterns of the composition Fe:Zr = 1:2 at various milling times starting from pure elemental powders. The peaks from pure elements are identified by labels 1 (Fe) or 2 (Zr) here and in Figs 2 and 3. Note that the y-scale for the pure elements is five times greater than for the other spectra.

where $\varrho_0 = [\Sigma_v n_i f_i(0)]^2/V$ and $M(s)$ is a modification function of the form

$$M(s) = \left\{1 \Big/ \left[\sum n_i f_i(s)\right]^2\right\} \exp(-ks^2)$$

with $k = 0.005$.

3. Results and discussion

Figs 1 to 3 show the amorphization process by MA for the composition $FeZr_2$ (Figs 1, 2) and Fe_2Zr (Fig. 3). Several points can be inferred from these figures.

(i) When starting from pure elements the amorphization process has been reached completely in about 20 h (Figs 1, 3). The milling time to promote amorphization is approximately the same as that reported by Hellstern and Schultz [12] who used the same planetary ball mill on iron–zirconium systems of similar compositions. Prolonged milling times do not substantially change the final product from a structural point of view. The hexagonal zirconium network (hcp) is much more sensitive to the deformation process than the cubic iron one (fcc) as shown by the more rapid disappearance of the zirconium lines (Figs 1 and 3).

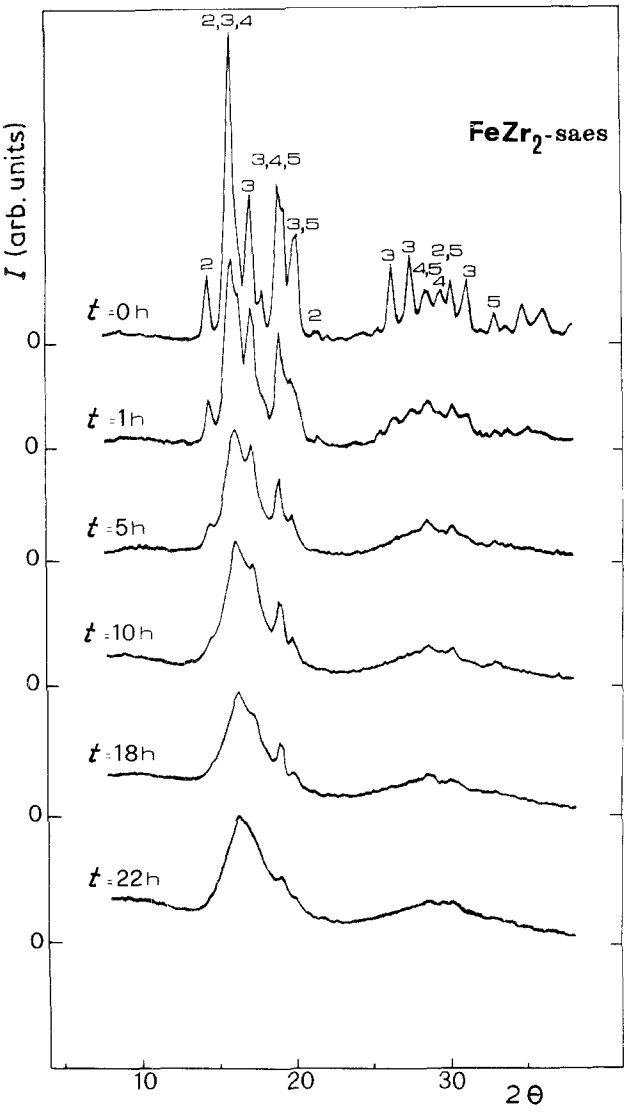

Figure 2 X-ray diffraction pattern of saes alloy (see text) at various milling times. (2) Zr peaks; (3, 4, 5) intermetallic compounds $FeZr_2$ (3, 4) and Fe_2Zr (5), respectively (see text).

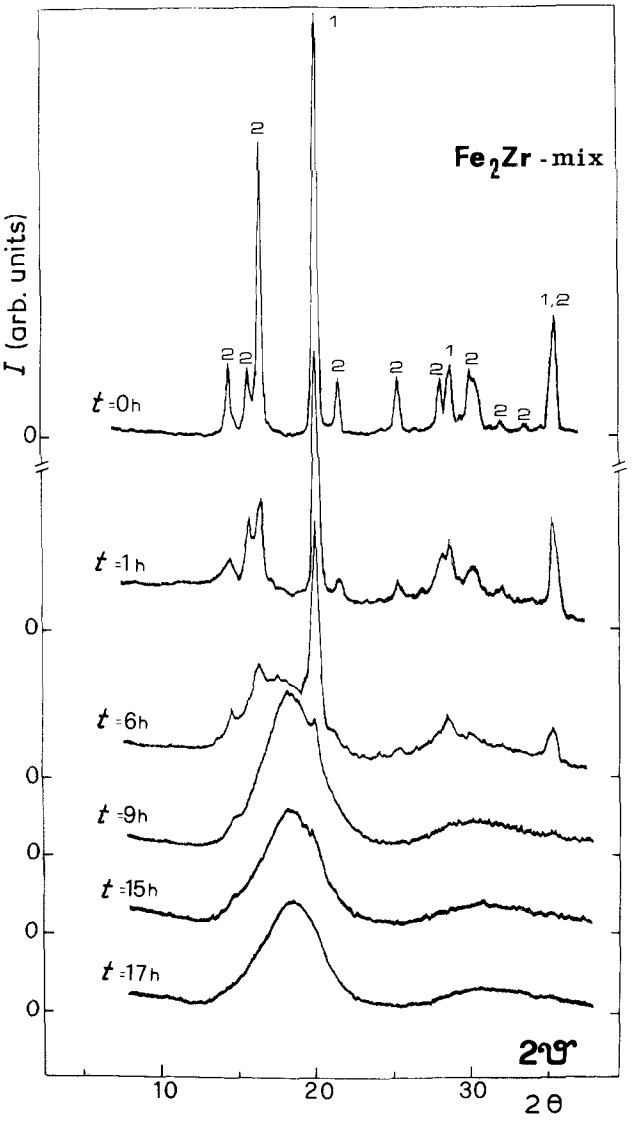

Figure 3 X-ray diffraction pattern of the composition Fe : Zr = 2 : 1 at various milling times starting from pure elemental powders.

(ii) When starting from $FeZr_2$-Saes alloy complete amorphization has not been reached (Fig. 2 shows milling time up to 22 h because prolonged milling up to 60 h does not eliminate the residual small peak at about 19°). A possible explanation lies in the presence, from the beginning, of stable intermetallic phases. The alloy has been prepared from the elements by usual fusion and casting procedures. Following the revised phase diagram given by Aubertin *et al.* [17], at room temperature only Fe_2Zr and $FeZr_3$ should be present. However, the peritectic reaction at 974° C between the primary crystallization product (Fe_2Zr) and the liquid to give $FeZr_2$ (further demixing at lower temperature) is incomplete. In fact the alloy is a non-equilibrium mixture in which several stable phases have been identified; namely two $FeZr_2$, tetragonal [18] and cubic [19] (labelled 3 and 4 in Fig. 2), a Fe_2Zr cubic phase [19] (5 in Fig. 2) and unreacted α-Zr (2 in Fig. 2).

The residual peak at about 19 after 22 h (or 60h) milling lies in the region where peaks from the intermetallic phases are more pronounced (see sequence 3, 4, 5 at $t = 0$ h in Fig. 2) thus suggesting that if a very stable intermetallic configuration is present it is difficult to promote complete amorphization.

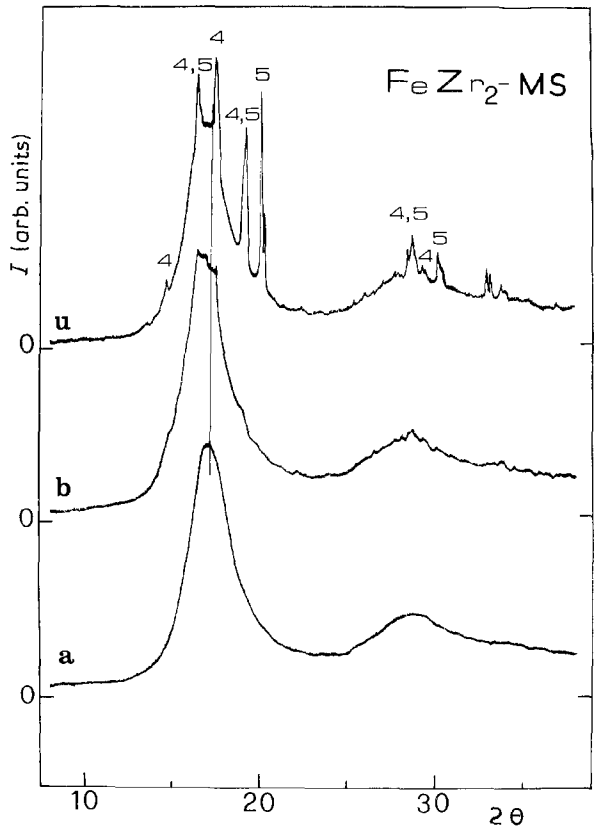

Figure 4 X-ray diffraction pattern of the melt-spun ribbon of Fe : Zr = 1 : 2 composition. (a) Completely amorphous ribbon (on both faces); (b), (u) bottom and upper face of a partially amorphous ribbon. (4, 5) Peaks of known compounds (see Fig. 2).

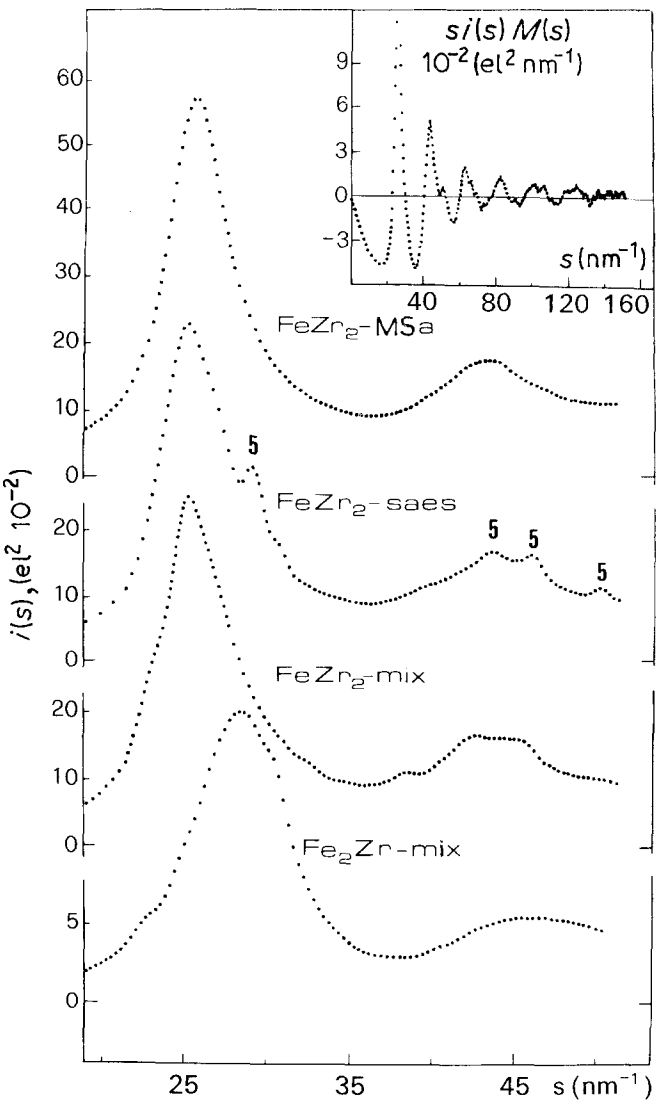

Figure 5 Scattered intensities in absolute units plotted against the scattering vector for four amorphous samples. The onset shows the structure function, in the $si(s)M(s)$ form, for the MSA sample.

In Fig. 5 (discussed further later), where quantitative data for four amorphous samples are reported, residual peaks on $FeZr_2$-saes have been identified as belonging to Fe_2Zr phase (label 5 in the figure). Following Miedema *et al.*'s [20] semiempirical model, ΔH values of -8.5 and -6.4 k cal mol^{-1} have been evaluated for the formation of the intermetallic Fe_2Zr and $FeZr_2$, respectively. Thus the more stable phase is indicated to be Fe_2Zr which is just the phase not completely disappearing when milling the saes alloy.

We have already detected the presence of small amounts of a stable crystalline phase (Pd_3Si) in equilibrium with a bulk amorphous $Pd_{80}Si_{20}$ obtained by MA from the elements [21]. Work in progress on that system indicates that even starting from the elements, once a very stable phase is formed (Pd_3Si in this case), it is quite difficult to promote complete amorphization. The problem lies in what is meant by "very stable" phase. In the light of the present knowledge, it should indicate a deep minimum of energy which cannot be increased, by the energy transfer of the milling process, in order to reach the higher energy level of the amorphous phase.

(iii) A third point worthy of mention is the different kinetic behaviour when starting from pure elements or from the alloy. In Fig. 2 the label for time $t = 0$ h is not strictly true, because the cast ingot has been already comminuted and a portion having about 100 mesh has been sieved as starting material. Thus for $t = 0$ h plastic deformations of the material have already been promoted. Nevertheless, a different kinetics in the amorphization process is clearly evinced by comparing Figs 1 and 2. Milling the alloy for 1 h immediately promotes amorphization, while milling the pure powders for the same time only gives a line broadening of the pure components. After 10 h, the difference is still evident, and only after 18 h do the two patterns become similar. As suggested by Schwarz [7] and evinced by Hellstern and Schultz [12, 13], the amorphization mechanism goes through the formation of elemental layers of the pure powders which favour either the atom mixing and/or a solid state interdiffusion reaction of the components. When starting from the alloy, the intimate mixing of the components is already existent and the energy transfer is active from the beginning to promote amorphization.

Let us now examine the samples prepared by the MS method. Fig. 4 shows the diffraction patterns of an $FeZr_2$ ribbon completely amorphous (a) and of another one, partially crystallized (b and u represent bottom and upper face of the same ribbon, the bottom face being the one in contact with the rotating wheel). The incomplete quenching in MSB and, even more, in MSU, allows the crystallization of Fe_2Zr (label 5) and $FeZr_2$ (label 4) intermetallic compounds. The presence in the crystallization products of a phase more iron-

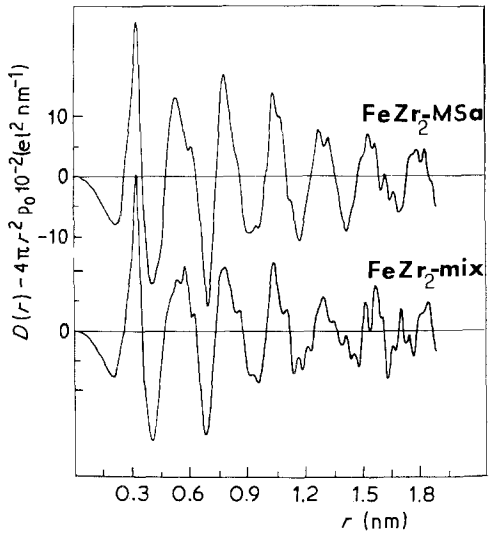

Figure 6 Radial distribution functions, in differential form $D(r) - 4\pi r^2 \varrho_0$, for two $FeZr_2$ samples prepared by MS (MSA) and MA (mix) methods, are shown in the interval 0 to 2 nm.

rich than the starting composition, indicates that the amorphous phase should be somewhat more zirconium-rich than the completely amorphous ribbon. The weak vertical line in Fig. 4 shows that the maximum of the first halo is slightly shifted towards smaller 2θ values in MSU with respect to MSA confirming an increased contribution of zirconium content in the former sample.

Fig. 5 shows the innermost parts of quantitative data taken from the melt-spun ribbon (MSA) and from the last stage of the mechanically alloyed samples of Figs 1 to 3. The onset shows the typical structure function in the whole angular range used to obtain the radial distributions functions. The maximum of the amorphous halo is centred at 25.8 nm^{-1} in MSA, 25.2 nm^{-1} in $FeZr_2$-saes and mix, and shifted towards 28.8 nm^{-1} in Fe_2Zr-mix reflecting the increased iron content. Fig. 6 shows the radial functions up to 2 nm for the two best amorphous samples of the same composition prepared via MS and MA, namely MSA and $FeZr_2$-mix. It may be seen that the estension of the order range, indicated by the presence of meaningful peaks, is around 1.5 to 1.8 nm in both cases. Further, the maxima positions are the same and their shapes are also similar, indicating a close structural arrangement in both samples.

A more accurate comparison is performed in Fig. 7 where only the first radial peak of the four amorphous samples is given. For the three $FeZr_2$ samples (MSA, saes, mix), difference curves have also been drawn to enhance the differences between the distribution functions. The maximum of the peak is centred at 0.318 nm (MSA), 0.320 nm (saes) and 0.323 nm (mix). The differences (MSA-saes) and (saes-mix) are so small that it is hard to attribute to them any real physical meaning. The (MSA-mix) difference is somewhat more enhanced and emanates from the 0.005 nm difference in the maxima positions of the radial curves. It might indicate a somewhat more expanded structure in the MA sample with respect to the MS sample. However, such a small variation is at the limit of confidence of the method [16]. As a matter of fact we can say that the

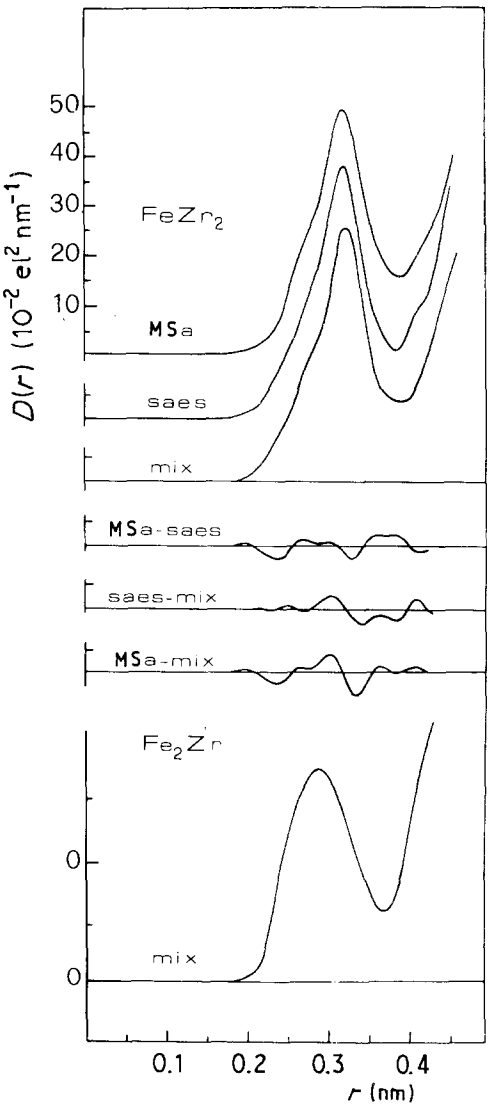

Figure 7 Distribution functions, in the $D(r)$ form, are shown for four amorphous samples. The first three from the top refer to samples of $FeZr_2$ composition (MSA, saes, mix). The fourth refers to Fe_2Zr. Difference curves between MS and MA samples (MSA-saes; MSA-mix) and two MA samples (saes-mix) are shown for a better comparison of the radial curves.

comparison gives a direct structural confirmation of the Mössbauer results of Michaelsen and Hellstern [15] who could not find structural differences between MA, MS and sputtered iron–zirconium samples.

As far as pair interactions contributing to the first peak are concerned, it is evident that the three peaks of the $FeZr_2$ samples are not symmetric and show a hump around 0.27 nm. On the basis of the radii of elements given by Egami and Waseda [22], Zr–Zr and Fe–Fe distances are expected to occur at 0.316 and 0.256 nm, respectively. The values perfectly match the features of the experimental radial peaks. The maximum may be ascribed to the longer Zr–Zr interactions, while the hump is explained by the shorter Fe–Fe distances. In the Fe_2Zr sample, in fact, the maximum is shifted to 0.288 nm reflecting indeed the great increase of the shorter Fe–Fe distances due to the different composition. In all cases, of course, Fe–Zr interactions also occur at distances included between those of the like elements. Table II shows the first neighbour distances existing in the known intermetallic $FeZr_2$ and Fe_2Zr compounds. It can be seen

TABLE II First neighbour distances found in intermetallic $FeZr_2$ and Fe_2Zr compounds

Compounds	Distances (nm)			
	Fe–Fe	Fe–Zr	Zr–Zr	Ref.
$FeZr_2$ (tetragonal)	0.280	0.275	0.312–0.356	[18]
$FeZr_2$ (cubic)	0.258	0.258, 0.303	0.303, 0.316	[19]
Fe_2Zr (cubic)	0.250	0.293	0.306	[19]

that the reported values are well in line with the experimental features of the radial curves of Fig. 7.

4. Conclusions

We have prepared amorphous iron–zirconium alloys by both MS and MA methods. The following points have been inferred.

1. Amorphous $FeZr_2$ samples have been obtained starting from either pure elemental powders or intermetallic compounds. Some differences, however, have been outlined concerning the kinetics of amorphization and the possibility of obtaining totally amorphous samples when starting from intermetallic compounds.

2. The structure of the melt-spun ribbon and mechanically alloyed samples is very similar in the meaningfully ordered region. The structural arrangement of the first neighbours around zirconium and iron atoms is indistinguishable in MS and MA samples.

Acknowledgements

We thank Drs M. Matricardi and A. Natalucci for assistance with some of the experimental work, and also A. Adriani for the analysis of the oxygen content in the samples.

References

1. J. S. BENJAMIN, *Metall. Trans.* **1** (1970) 2943.
2. P. S. GILMAN and J. S. BENJAMIN, *Ann. Rev. Mater. Sci.* **13** (1983) 279.
3. C. C. KOCH, O. B. CAVIN, C. G. MCKAMEY and J. O. SCARBROUGH, *Appl. Phys. Lett.* **43** (1983) 1017.
4. W. L. JOHNSON, *Prog. Mater. Sci.* **30** (1986) 81.
5. S. ENZO, L. SCHIFFINI, L. BATTEZZAT and G. COCCO, Proceedings of the Conference on Solid State Amorphizing Transformations, 1987, Los Alamos National Laboratory, to appear in *J. Less Common Metals* **140** (1988) 129.
6. R. SUNDARESAN and F. H. FROES, *J. Metals* **39** (1987) 22.
7. R. B. SCHWARZ, R. R. PETRICH and C. K. SAW, *J. Non-Cryst. Solids* **76** (1985) 281.
8. J. R. THOMPSON and C. POLITIS, *Europhys. Lett.* **3** (1987) 199.
9. K. M. J. BUSCHOW, *J. Less Common Met.* **79** (1981) 243.
10. *Idem, J. Phys. F Met. Phys.* **14** (1984) 593.
11. Z. ALTOUNIAN, C. A. VOLKERT and J. O. STROMOLSEN, *J. Appl. Phys.* **57** (1985) 1777.
12. E. HELLSTERN and L. SCHULTZ, *Appl. Phys. Lett.* **48** (1986) 124.
13. *Idem, ibid.* **49** (1986) 1163.
14. *Idem, Phil. Mag. B* **56** (1987) 443.
15. C. MICHAELSEN and E. HELLSTERN, *J. Appl. Phys.* **62** (1987) 117.
16. M. MAGINI, G. LICHERI, G. PICCALUGA, G. PASCHINA and G. PINNA, in "X-ray diffraction of ions in aqueous solutions: Hydration and Complex Formation", edited by M. Magini (CRC, Boca Raton, Florida, 1988) Ch. 1.
17. F. AUBERTIN, U. GONSER, S. J. CAMPBELL and H. J. WAGNER, *Z. Metallkde* **76** (1985) 237.
18. E. E. HAVINGA, H. DAMSMA and P. HOKKELING, *J. Less Common Met.* **27** (1972) 169.
19. R. M. VAN ESSEN and K. H. J. BUSCHOW, *ibid.* **27** (1972) 277.
20. A. R. MIEDEMA, P. F. DE CHATEL and F. R. DE BOER, *Physica* **100B** (1980) 1.
21. M. MAGINI, S. MARTELLI and M. VITTORI, *J. Non-Cryst. Solids* **101** (1988) 294.
22. T. EGAMI and Y. WASEDA, *ibid.* **64** (1984) 113.

Received 11 August 1988
and accepted 2 January 1989